Experimental study of solid-liquid-type transitions in vibrated granular layers and the relation with surface waves

Nicolás Mujica and Francisco Melo
Departamento de Física de la Universidad de Santiago de Chile, Avenida Ecuador 3493, Casilla 307 Correo 2 Santiago, Chile
(Received 26 July 1999; revised manuscript received 7 March 2000; published 19 December 2000)

From pressure and surface dilation measurements, we show that a solid-liquid-type transition occurs at low excitation frequencies in vertically vibrated granular layers. This transition precedes subharmonic bifurcations from flat surface to standing wave patterns, indicating that these waves are in fact associated with the fluidlike behavior of the layer. At higher frequencies we show that another kind of subharmonic waves can be distinguished. These waves do not involve any lateral transfer of grains within the layer, and correspond to excitations for which the layer slightly bends alternately in time and space. These bending waves have very low amplitude, and we observe them in a vibrated two-dimensional layer of photoelastic particles.

DOI: 10.1103/PhysRevE.63.011303 PACS number(s): 45.70.−n, 45.70.Qj, 83.80.Fg

I. INTRODUCTION

In a driven granular system, such as a vibrated layer composed of macroscopic particles, energy is dissipated by inelastic collisions and by friction. Also, for realistic situations, the typical energy of a grain is many orders of magnitude greater than k_BT, so the temperature does not play an important role in the dynamics of these materials. However, it is commonly observed that granular matter behaves like solids, liquids, or even gases depending on the energy injection and energy dissipation rates [1]. More precisely, the steady-state balance between these rates determines the residual velocity fluctuations, which in turn play the role of thermal fluctuations in these materials.

Surface waves excited by vertical vibrations provide one of the most striking examples in which granular materials act like a fluid. For a granular layer, it was found that parametric waves can be observed whenever the dimensionless acceleration $\Gamma = A(2\pi f)^2/g$ exceeds a critical value [2] (here g is the acceleration of gravity, A is the amplitude of the vibrating surface, and f is the frequency of the driving force). The primary instability resulted in a transition from a flat layer to a pattern of squares or stripes, depending on both f and the particle diameter d. As an illustration we present two typical snapshots of these kinds of waves in Figs. 1(a) and 1(b). It was found that the crossover frequency f_d at which a square to stripe transition occurs is proportional to $d^{-1/2}$. In addition, this scaling can be qualitatively understood in terms of the ratio of kinetic energy injected into the layer to the potential energy required to raise a particle a fraction of its diameter. At low f, the horizontal mobility should be high since the layer dilation is large [3,4], whereas at large f, the mobility should be low since the layer dilation is small [5]. We note, however, that these waves are the corresponding hydrodynamic surface modes of the layer, since they require a transfer of mass to be sustained [2,4,5].

In this paper, we report on measurements of the pressure due to the layer-container collision and the surface and bulk dilation of the layer. We show that there exists a critical Γ for which the flat layer undergoes a phase transition. This critical Γ is smaller than the critical one at which waves appear. At low f this transition is a solid-liquid type, at intermediate f only a heating up of the surface layer is observed, whereas at high f a compaction crossover is detected. Thus our results show that granular surface waves are naturally linked to fluidlike behavior, since they are observed only when the energy input per particle is enough to induce a minimal dilation of the flat layer. At high f and for the same critical value of Γ at which hydrodynamic waves appear, bending waves are detected instead. In this regime, our measurements show that the mobility of grains is almost completely suppressed in both the bulk and the free surface of the layer. In this case, a set of experiments conducted with large photoelastic particles allows us to observe these waves as an alternation of bright and dark zones that oscillate in time at half of the forcing frequency. In addition, we show for the low-frequency regime that when Γ is increased to a value close to 4.6, an inverse transition from a fluid to a compact layer is observed. This transition is responsible for the flat with kinks state reported in previous works [2] [see Figs. 1(c) and 1(d)]. A brief summary of our results was given in Ref. [5].

This paper is organized as follows: Section II is devoted to the description of our experimental setup. In Sec. III we present our pressure measurements and we establish the basis to obtain density profiles and the bulk dilation from the experimental data. In Sec. IV we present surface dilation measurements, and we discuss how they link to the bulk dilation measurements. The energy dissipation rate in the vibrated layer is also estimated as a function of the excitation frequency. Section V is concerned with a study of the very low amplitude regime of surface waves, and its connection with the compact state of the layer. Finally a brief discussion is given.

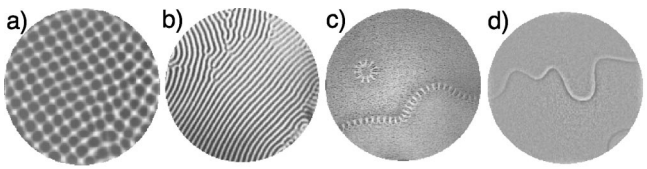

FIG. 1. Snapshots of the layer state at differents conditions obtained in a large cell. (a) Squares, $f \sim 20$ Hz, $\Gamma = 3.0$. (b) Stripes, $f \sim 60$ Hz, $\Gamma = 3.0$. (c) Flat with kinks at $f \sim 25$ Hz, $\Gamma = 4.7$. (d) Flat with kinks at $f \sim 60$ Hz, $\Gamma = 4.7$.

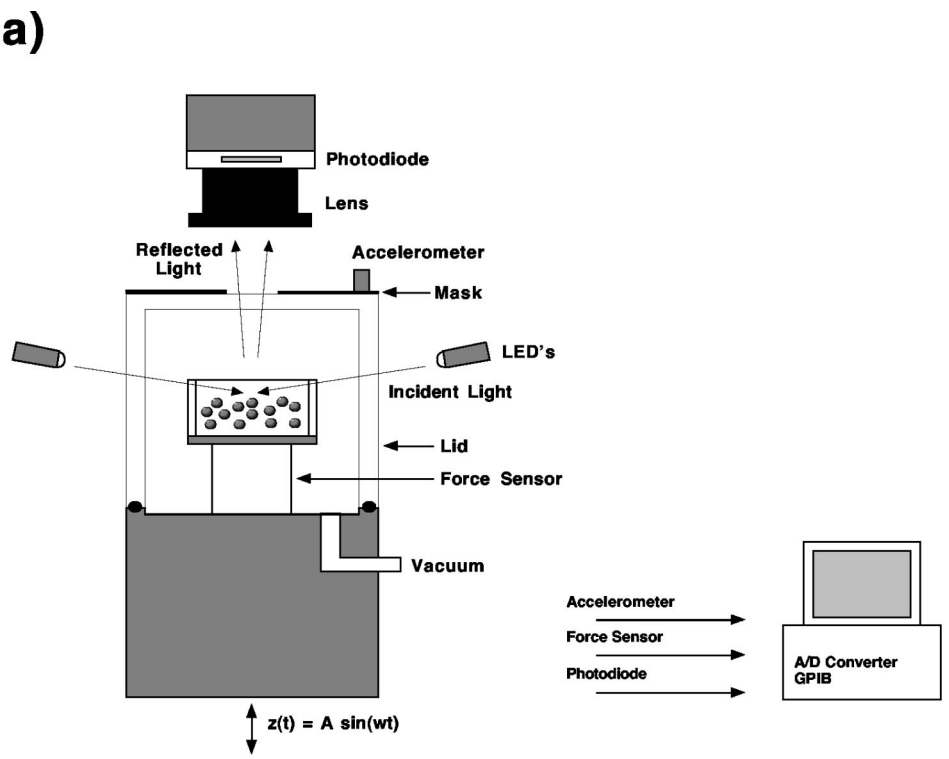

FIG. 2. Schematic drawings of (a) the experimental setup showing the cylindrical cell, the location of the pressure sensor, and the setup for reflectivity measurements; and (b) a fluidized granular layer, where α is the angle of incidence and the white particles are those which compose the effective surface layer.

II. EXPERIMENTAL SETUP

In this paper we present two sets of experiments. In the first set, we simultaneously measure the pressure resulting from the collisions of the layer with the vibrating plate, and the surface particle dilation. From the pressure measurements, we obtain information on the bulk dilation and density (Sec. III). The surface dilation is determined through the normalized reflected intensity of the surface layer (see the discussion below).

In Fig. 2(a) we present a schematic drawing of the experimental setup. In this experiment, a thin layer of $d = 0.106–0.125$ mm diameter bronze particles, 15 particles deep, is placed at the bottom of a 40-mm-diameter and 25-mm-height cylindrical container. The container's wall is Lucite, while the base is aluminum to reduce electrostatic effects. The container is mounted on a high-frequency response pressure sensor (PCB. Model 208A11) which is driven by an electromechanical vibration exciter. The resulting acceleration is measured to a resolution of $0.01g$. A second Lucite cylinder is used as a lid for the whole system, allowing evacuation of the container to less than 0.1 Torr; at this value volumetric effects of the gas are negligible [6]. The surface of the layer is illuminated at low angle (20° with respect to the horizontal) by an array of 18 light emitting diodes organized in a 10-cm-diameter ring. The reflected light from the surface layer is focused by a lens of 28-mm focal length on a flat photodiode of 25-mm^2 area. The lens aperture angle is about 12°. The whole system is automatically run by a Power PC computer equipped with analog-to-digital converter (A/D) and general purpose interface bus (GPIB) boards.

With this setup, the measured intensity I is proportional to both the incident intensity of light I_i and the reflectivity coefficient of the bronze particles R ($R \sim 0.6$). In fact, we can write I in the form

$$I \approx N^* \bar{s} R I_i , \tag{1}$$

where N^* is the number of particles that reflect light to the sensor, and $\bar{s}$ is a geometrical factor. There are several points that must be discussed.

(i) The physical meaning of N^*. In Fig. 2(b) we show a schematic view of the granular layer in a fluidized state. One way to characterize the granular layer is by defining an effective surface layer as the set of particles that have a high probability to be illuminated by a beam of light. We can also define an average separation between grains δ_s, the surface dilation, as the average separation between the nearest neighbors of this effective surface layer. In Fig. 2(b) the particles marked in white are those which belong to what we call the effective surface layer. As the incident angle α is small (respect to the horizontal), the probability for a ray of light to go through this effective surface layer is very small. In fact, if δ_s is the distance between two particles of the surface layer (which are nearly in the same horizontal plane), then a ray would be able to go through only if $\alpha > \alpha^*$, where $\sin(\alpha^*) = d/(\delta_s + d)$. This gives us a condition for a critical dilation δ_s^*; for surface dilations smaller than this value, no rays can directly reach inferior layers. For $\alpha \approx 20°$, we find $\delta_s^* \approx 2d$. Compared with our experiments this value is quite high, and it would only be achieved for strong fluctuations of the surface dilation; on average, the induced dilation is much lower than this value (see Secs. III and IV). Another important point is that in the case that a ray could reach an inferior layer, it seems even less probable that its reflection would be able to reach the photodiode without being scattered by another particle. Finally, we note that in the image of the vibrated granular layer presented in Fig. 2(b) we have assumed *local isotropy*; in this sense the effect of strong fluctuations of the surface dilation is considered to be small. Therefore, we finally conclude that N^* is mainly given by the number of particles in the effective surface layer.

(ii) The efects of multiple reflections. For a first reflection, we note that on a single particle only a small ring reflects light in the direction of the solid angle of the lens. The surface of this ring is a small fraction of the total surface of a particle, namely, $s \approx 0.05$. Thus we neglect multiple reflections, since their dominant contribution is proportional to both R^2 and s^2, where s^2 represents the probability of having a secondary reflection within the solid angle of the camera.

(iii) The meaning of $\bar{s}$. Considering the previous points and energy conservation we conclude that $\bar{s}$ is the area of one particle that reflects light into the photodiode divided by the area of the photodiode.

The intensity I, measured by the photodiode, can be then taken to be proportional to the number of particles within the surface layer, or more precisely to the surface density ρ_s,

$$I \approx \rho_s A_o \bar{s} R I_i , \tag{2}$$

where A_o is the area of observation (~ 1 cm^2), and $\rho_s = N^*/A_o$. Then we can relate I to the surface dilation δ_s through the definition

$$\rho_s = \frac{\bar{\nu}}{(d+\delta_s)^2}, \tag{3}$$

where $\bar{\nu}$ is an average coordination number that takes into accout the disorder [3]. Thus we finally obtain the normalized reflected intensity

$$\frac{I}{I_o} \approx \frac{d^2}{(d+\delta_s)^2}, \tag{4}$$

where I_o is a reference intensity for which we take $\delta_s = 0$. Experimentally I_o is measured after a ''fluidization'' of the layer, for many cycles, at $\Gamma = 2.4$ and $f = 40$ Hz. Before each measurement we set the initial state of the layer by this procedure. This initial state is not the most compact one accessible for the layer, so we can say that the initial state has a characteristic roughness or, what is equivalent, a characteristic initial surface dilation (which should be small). Thus the choice $\delta_s = 0$ for $I = I_o$ is just a reference value. We finally remark that Eq. (4) is valid for homogenous layers (for layers that have not undergone a subharmonic wave instability).

The second set of experiments consists of vibrating a two-dimensional layer of photoelastic particles and taking images of the layer motion with a high speed charged-coupled-device (CCD) camera. The goal is to observe the very low amplitude waves found in the high frequency regime. A cell made of two glass plates 400 mm wide by 100 mm high was mounted on the moving platform of our vibrator system. The gap between the plates is controlled by spacers of varying thickness to a resolution of 0.05 mm. Images with resolution of 256×256 pixels are captured at rates of 1200 frames per second by a Hisis 2002 CCD camera. Images are obtained by transmission using parallel light with incidence perpendicular to the cell. Transmitted light is filtered through a polarizer whose axis is perpendicular to direction of polarization of the incident light. More details are given in Sec. V.

III. PRESSURE MEASUREMENTS AND DENSITY PROFILES

A. Experimental procedures and collision model

In Fig. 3(a) we present a typical pressure signal $P(t)$ as a function of time for $f = 40$ Hz and $\Gamma = 2.2$. This signal is composed of a sinusoidal component, corresponding to the force required to accelerate the cell, and of a peak sequence, due to the layer-plate collisions. We are interested in the shapes of the peaks during the collision, so it is necessary to subtract the sinusoidal component. Then, from the pressure signal, we obtain several pressure peaks, typically between 15 and 20, which only represent the pressure exerted on the plate during the collisions. As an illustration of this procedure, in Fig. 3(b) we present the average peak obtained from the peaks presented in Fig. 3(a). To characterize the peaks of a sequence like the one presented, we take the maximum

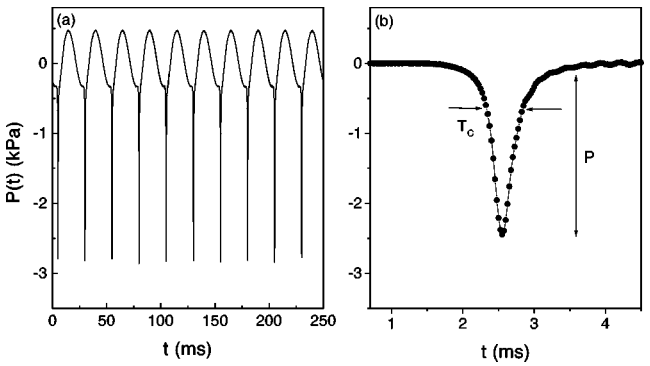

FIG. 3. (a) Time evolution of the pressure signal $P(t)$ for $f=40$ Hz and $\Gamma=2.2$. In (b) we present the averaged collision peak obtained from $P(t)$, and we show the definition of the maximum pressure P. The collision time T_c is the width of the peak at certain height.

value P and the width T_c, which is a measure of the collision time. More precisely these quantities are obtained as the averages of the sequence $\{P^{(k)},T_c^{(k)}\}$, where k is an integer that indicates the collision number, i.e., $P=\langle P^{(k)}\rangle$ and $T_c=\langle T_c^{(k)}\rangle$ where $\langle\ \rangle$ denotes the sequence average. For the data in Fig. 3, $P=2.45\pm0.03$ kPa and $T_c=0.52\pm0.01$ ms. (In this case T_c is taken as the width at a pressure equal to a quarter of P.)

Now, due to the impulsive nature of the layer plate collision, we write the scaling relation

$$P\sim\frac{M}{A_p}\frac{V_c}{T_c}, \tag{5}$$

where M is the total mass of the layer, A_p is the active surface of the plate, and V_c is the layer-plate relative velocity at the collision. If the collision takes place at a time $t=\overline{t}$ and is completely inelastic, then $V_c=V_p(\overline{t})-V_b(\overline{t})$, where V_p and V_b are the plate and layer velocity, respectively. Thus, in practice, we approximate the collision velocity by the one predicted by the completely inelastic ball model. We note that this model assumes that the layer immediately loses all its energy and takes on the velocity of the moving plate. This is an idealization; what is true is that the energy of the layer is almost completely lost before the next takeoff [2,7]. Thus what is well approximated is the velocity of the takeoff, and thus the relative velocity at the collision. This approximation is valid since previous experiments showed, by measuring the flight time of the layer, that the motion of the center of mass of the layer follows the motion of an inelastic ball [2,7].

We remark that in our experiments, even close to $\Gamma\sim1$, the vertical average bulk dilation of the layer, δ_b, is never strictly zero. This is concluded because the collision time is not determined by the Hertz theory. Indeed, experiments performed by Falcon *et al.* [8] showed that, in the case of a column of N particles in contact ($\delta_b=0$) colliding vertically with a fixed plate, the collision time is $T_c=(N-1)T_q+\tau_1$, where N is the number of particles, T_q is the time duration of the momentum transfer from one particle to another, and τ_1 is the collision time between two particles predicted by Hertz theory [9]. Now, for the particles used in our experiments, the orders of magnitude of these times are $T_q\approx\tau_1\approx10^{-6}$ s [10]. Then the predicted collision time for our three-dimensional layer should be of order $T_c\approx10^{-5}$ s. Nevertheless, in our experiments the minimum collision time observed is of order $T_c\approx5\times10^{-4}$ s (for $\Gamma\sim1$, and for a wide range of f). The difference between what is expected from the Hertz prediction for $\delta_b=0$ and the experimental values for T_c can be explained if the layer is slightly dilated at the collision; a local dilation of 1% ($\delta_b/d\sim0.01$) drastically changes the collision regime from the Hertz contact to ballistic collisions. Although this effect has interesting consequences on sound propagation, it does not affect the center of mass motion of the layer. Thus, for $\Gamma>1$, we write the total dilation of the layer as $\Delta=V_cT_c$. If, in addition, we assume that dilation is homogeneous, i.e., $\Delta=N\delta_b$, where N is the number of layers, we can write Eq. (5) as

$$P\sim\frac{M}{A_p}\frac{V_c^2}{N\delta_b}. \tag{6}$$

Thus our procedure to measure the local bulk dilation δ_b is the following: we fit P versus V_c/T_c to obtain the numerical factor of Eq. (5), and we then use Eq. (6) to obtain the value of δ_b.

In the following, we will relate the layer density to the pressure signal $P(t)$. Figure 4 presents a schematic view of a collision. We consider that the plate collides with the granular layer of density $\rho(z)$ at a velocity V_c at time $t=0$. Then, the layer is initially fixed in space, and the plane $(x,y,z=0)$ of the reference frame (x,y,z) coincides with the bottom layer just before the collision [see Fig. 4(a)]. We also note that the mass of the plate M_p is much larger than the mass M of the layer ($M/M_p\sim0.01$), so we neglect any velocity change of the plate due to momentum transfer. We also neglect the variation of the relative velocity due to the action of gravity, since experimentally we observe that $gT_c\ll V_c$. Thus the force exerted on the plate due to momentum transfer is

$$F(t)\approx\frac{dm(t)}{dt}V_c. \tag{7}$$

Here $m(t)$ is the mass that has collided with the plate at time t. Next we need to link $dm(t)/dt$ to $\rho(z)$, measured in the fixed frame (x,y,z). To do this we define the compression front $z_c(t)$ as the height (relative to the fixed frame) of the mass that has been deposited on the plate at time t [see Fig. 4(b)]. We assume that all the compaction is occurring at the compression front, which is a reasonable approximation. Then the mass $m(t)$ accumulated on the plate becomes

$$m(t)=A_p\int_0^{z_c(t)}\rho(z)dz, \tag{8}$$

whose derivative with respect to time is

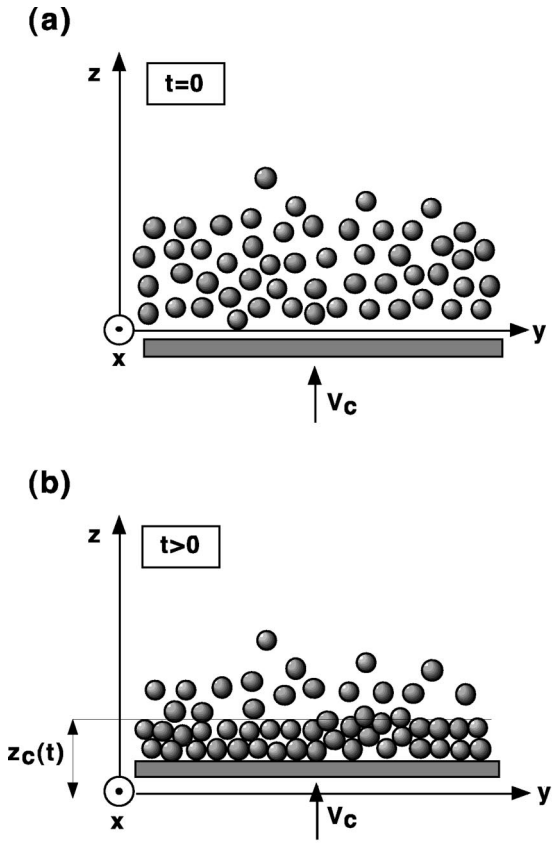

FIG. 4. Schematic of the collision. (a) shows the instant $t=0$ at which the plate colides with the layer. The velocity of the collision is V_c, and the density of the layer before the collision is $\rho(z)$. (b) shows how the layer accumulates over the moving plate at an instant $t>0$. We also present the definition of $z_c(t)$ as the position of the compresion front relative to the origin of the fixed frame (x,y,z). In all the calculations the effect of gravity is neglected, since experimentally $gT_c \ll V_c$.

$$\frac{dm(t)}{dt} = A_p \rho[z_c(t)] \frac{dz_c(t)}{dt}. \tag{9}$$

Now, at time t, the plate has moved a distance $V_c t$ from its initial position, and the height of the layer with respect to the plate can be written

$$h(t) \equiv \frac{m(t)}{A_p \rho_o} = \frac{1}{\rho_o} \int_0^{z_c(t)} \rho(z) dz, \tag{10}$$

where ρ_o is the mass density of the layer in the compact state. We then obtain

$$z_c(t) = V_c t + \frac{1}{\rho_o} \int_0^{z_c(t)} \rho(z) dz. \tag{11}$$

Differentiating this equation with respect to time, we obtain the density evaluated at the location of the compression front as a function of its velocity $\dot{z}_c(t)$:

$$\rho[z_c(t)] = \rho_o \left(1 - \frac{V_c}{\dot{z}_c(t)} \right). \tag{12}$$

Using this result in Eq. (9), relation (7) for the force becomes

$$\frac{F(t)}{A_p \rho_o V_c} = \dot{z}_c(t) - V_c. \tag{13}$$

Integrating this equation between 0 and t gives an expression for the compression front as a function of time:

$$z_c(t) = V_c t + \frac{1}{A_p \rho_o V_c} \int_0^t F(\bar{t}) d\bar{t}. \tag{14}$$

In summary, from the pressure signal $P(t)=F(t)/A_p$, we deduce the time evolution of the compression front $z_c(t)$. Also, we use Eq. (12), which tells us about the time evolution of the density at the compression front. Since the time t enters as a simple parameter, we can obtain the density as a function of z_c, right before the collision.

Finally, we note that both Eqs. (12) and (13) are laws for the conservation of mass and momentum through the compression front. It is possible to deduce from them the velocity of the compression front and the pressure in the compressed part of the layer as implicit functions of $\rho[z_c(t)]$:

$$\dot{z}_c(t) = \frac{\rho_o V_c}{\rho_o - \rho[z_c(t)]},$$

$$\frac{F(t)}{A_b} = \frac{\rho_o \rho[z_c(t)] V_c^2}{\rho_o - \rho[z_c(t)]}.$$

These expressions are generalizations of those obtained by Goldshtein *et al.* [11] for the propagation of a shock wave through an homogeneous layer of inelastic particles.

Before presenting our experimental results we will show that with Eq. (14) we can check the momentum conservation of the collision. Evaluating it at time $t=T_c$ (here T_c is the total collision time), we obtain

$$z_c(T_c) = V_c T_c + \frac{1}{A_p \rho_o V_c} \int_0^{T_c} F(\bar{t}) d\bar{t}. \tag{15}$$

Since by definition $z_c(T_c)=H+V_c T_c$, where H is the layer thickness in the compact state and $V_c T_c$ is the total displacement of the plate during the collision, and $\rho_o = M/HA_p$, we find

$$\int_0^{T_c} F(\bar{t}) d\bar{t} = M V_c. \tag{16}$$

B. Experimental results

We begin this section by presenting results concerning the momentum conservation relation [Eq. (16)]. Experimentally we have checked this for a wide range of parameters, namely, $1<\Gamma<\Gamma_w \approx 2.8$ and 35 Hz$<f<$350 Hz (Γ_w is the onset for parametric waves). The main point is that, in our experiment, the velocity V_c calculated from the completely

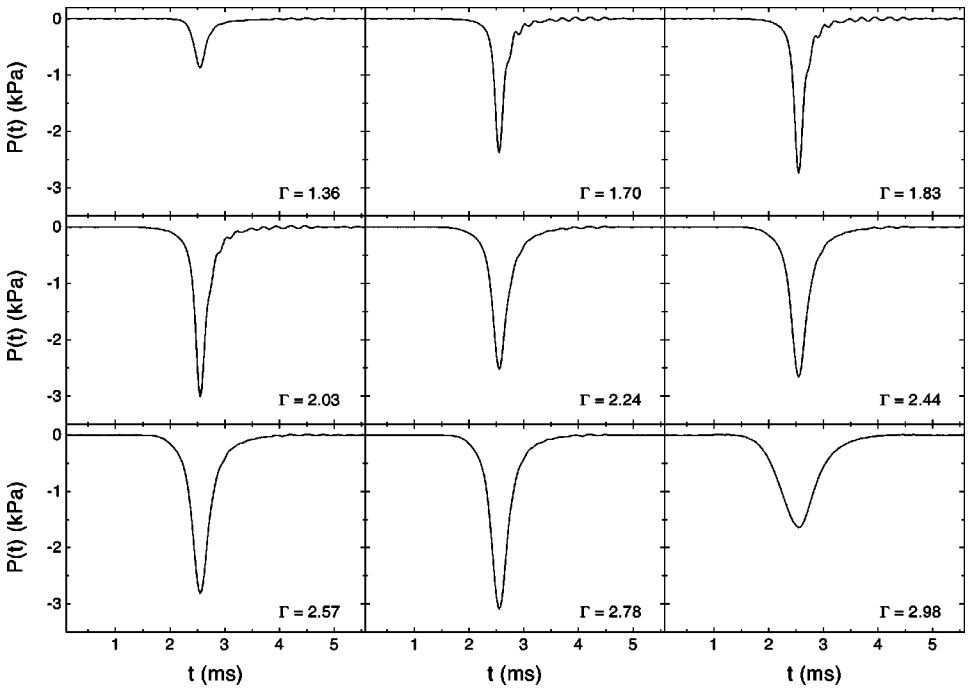

FIG. 5. Averaged pressure peaks as functions of time for various values of Γ and $f=40$ Hz. For $\Gamma=2.98$ the layer is already in the wave regime.

inelastic ball model is a very good approximation. As the internal degrees of freedom of the layer are excited, one expects that this approximation becomes less accurate. However, this only occurs in the wave regime where the takeoff velocity is reduced, and then both the collision velocity and the flight time are smaller than predicted [2].

There are other experimental effects that should be considered. For instance, friction on the cell walls can transfer momentum to the layer. Another posibility, much less probable, is the transfer of momentum to the walls by the formation of dynamical arcs. Therefore, taking into account these sources of errors and those due to mass measurement and acceleration and pressure sensor calibration, we expect that the correct form of the momentum conservation to be

$$\int_0^{T_c} F(\bar{t})d\bar{t}=M_{eff}V_c, \tag{17}$$

where M_{eff} is an effective mass, and V_c is the velocity of collision calculated from the completely inelastic ball model. From this model, we know that $V_c=gF(\Gamma)/f$, where $F(\Gamma)$ is a nonanalytic function of Γ, which is found numerically [7]. From our data we then find that the scaling $\int_0^{T_c}F(\bar{t})d\bar{t}\sim V_c$ is very well verified as a function of both Γ and f. As expected, we find that M_{eff} is constant and it is about 10% lower than M.

In order to complete our description, it is necessary to estimate the granular density in the compact state ρ_o. This quantity is in principle a dynamical variable, in the sense that it depends on how we compact our layer. However, we note that the important parameter in Eq. (14) is $A_p\rho_o=M/H$. Taking into account the previous discussion about the effective mass of the layer and that $H\approx 1.7$ mm, we obtain $A_p\rho_o\approx 4.2$ kg/m. Finally, for the force integration in Eq. (14), we define T_c as the width of the pressure peaks at $\frac{1}{20}$ of P. The results obtained are not sensitive to this cutoff.

Figure 5 presents averaged pressure peaks for several values of Γ at $f=40$ Hz. Each curve is obtained as an average of the pressure peaks of a pressure time series, in the same way that for the curve presented in Fig. 3(b). We note that our analysis is valid for cases for which $\Gamma<\Gamma_w\approx 2.8$. Thus the last pressure curve presented for $\Gamma=2.98$ is shown to display the difference of the parametric wave state; at this value of Γ the collision is quite spread out in time, and the maximum pressure achieved is also much smaller . We will discuss this point more in Sec. IV. For all the other pressure curves presented, except around $\Gamma\sim 2$, the intensity of the collision seems to be an increasing function of Γ, i.e., the maximum pressure P increases. In a first order description we understand this as the simple fact that the relative velocity of the collision V_c is increasing with Γ, as it does in this region of Γ in the completely inelastic ball model. What is not possible to explain with this model are the facts that P slightly decreases after $\Gamma\sim 2$, and that the collision time T_c also seems to be an increasing function of Γ. As discussed, these observations are related to the excitation of the internal degrees of freedom of the granular layer, i.e., the layer is dilated (see below).

In Fig. 6 we present the layer density as a function of height for each of the curves introduced in Fig. 5. In general, the density $\rho(z)$ is approximately constant in a center region, and decreases toward both ends of the layer. A penetration length for the dilation of the layer can be identified. This length increases with Γ; for instance, it is of the order of d and $3d$ for $\Gamma\approx 1.4$ and 2.4 respectively. Another fact that traces back the dilatancy of the layer is that its thickness increases with Γ; it is $14d$ for $\Gamma\approx 1.4$ and $17d$ for $\Gamma\approx 2.8$. In the limit of $\Gamma\sim 1$ we obtain that the density in the central part of the layer is close to ρ_o.

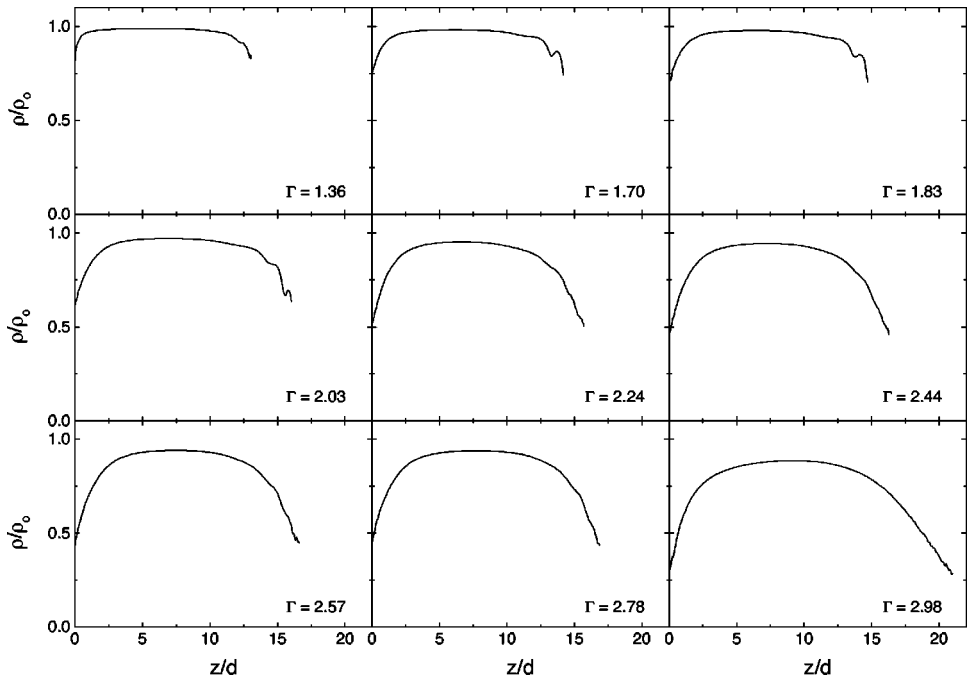

FIG. 6. Normalized density $\rho(z)/\rho_o$, as a function of height z, for various values of Γ and $f=40$ Hz.

Another interesting piece of information is the bulk dilation within the layer, δ, as a function of z. This quantity is linked directly to the density as $\rho(z)=\overline{\nu} m_o/(d+\delta)^3$, where $\overline{\nu}$ is an average coordination number and m_o the particle mass [3]. Defining $\delta=0$ for $\rho(z)=\rho_o$, we obtain

$$\frac{\delta(z)}{d}=\left(\frac{\rho(z)}{\rho_o}\right)^{-1/3}-1. \tag{18}$$

Then, it is possible to find $\delta(z)$ for all the data presented previously, which is shown in Fig. 7. From this figure, we can qualitatively examine the dependence of $\delta(z)$ on Γ, as we did for $\rho(z)$. For instance, as we increase Γ, the top and bottom of the layer continuously dilate and the extension of the dilated part increases. The central part also dilates as Γ increases; for $\Gamma\approx 1.4$ and $\Gamma\approx 2.4$ it is of the order of $0.004d$ and $0.02d$, respectively. We also note that for $\Gamma\approx 2.4$, the value $\delta\approx 0.1d$ is reached for $z\approx 2d$ and $z\approx 15d$, while the total height of the layer is approximately $17d$.

At this point, it seems appropriate to define a quantity as the vertical average of $\delta(z)$; we do this because it is necessary to link it in some way to δ_b. Therefore, we define this average dilation as

$$\langle\delta\rangle=\frac{1}{H'}\int_0^{H'}\delta(z)dz, \tag{19}$$

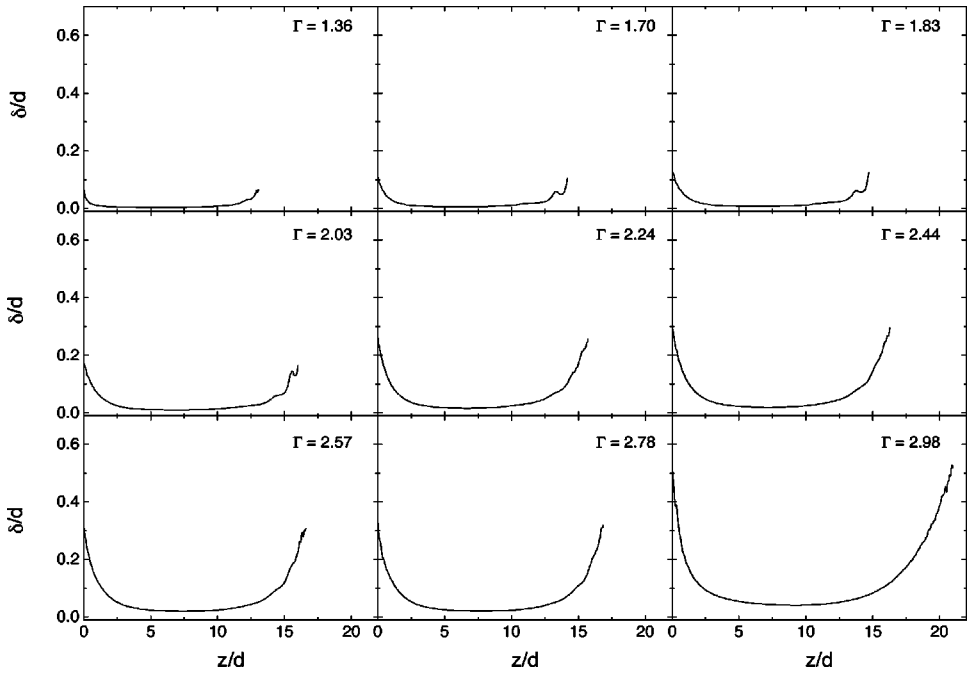

FIG. 7. Normalized dilation $\delta(z)/d$, as a function of height z, for various values of Γ and $f=40$ Hz.

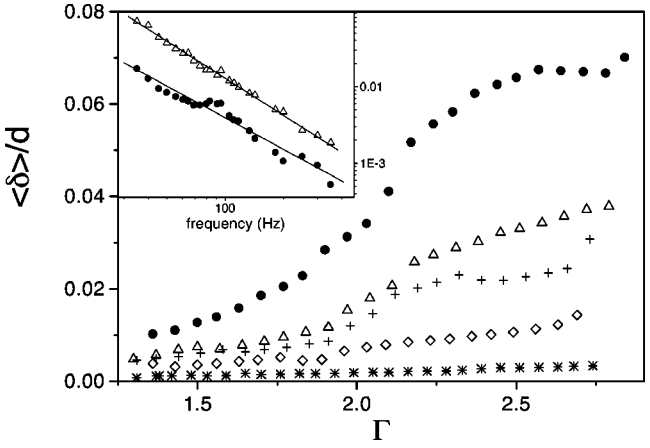

FIG. 8. Normalized average dilation $\langle\delta\rangle/d$, vs Γ for various values of f:(●) $f=40$ Hz, (△) $f=55$ Hz, (+) $f=70$ Hz, (◇) $f=120$ Hz, and (*) $f=250$ Hz. In the inset, we show the log-log plot of $\langle\delta\rangle$ vs f for $\Gamma=1.5$ (●) and 2.4(△). The continuous lines show the fits $\langle\delta\rangle=af^b$ for each Γ, with $a=0.35\pm0.12$, $b=-1.38\pm0.06$ and $a=1.27\pm0.05$, $b=-1.58\pm0.03$, respectively.

where H' is the total height of the layer. Note that H' depends on the excitation intensity (i.e., it depends on Γ and f).

Figure 8 presents $\langle\delta\rangle$ versus Γ for several excitation frequencies. In the low frequency regime we observe that $\langle\delta\rangle$ increases by a factor 3 around $\Gamma\approx2$. In contrast, at high f this increase has a tendency to disappear, and we observe that $\langle\delta\rangle$ is roughly a linear function of Γ. Complementing the previous data, in the inset of Fig. 8 we present $\langle\delta\rangle$ versus f for two values of Γ, below and above $\Gamma=2$. The average dilation $\langle\delta\rangle$ is a decreasing function of f. We also present with continuous lines the fits $\langle\delta\rangle\sim f^b$; we find $b=-1.38\pm0.06$ and $b=-1.58\pm0.03$ for $\Gamma=1.5$ and $\Gamma=2.4$, respectively. Similar behaviors are obtained for δ_b, as functions of both Γ and f (see Sec. IV).

To conclude, in this section we presented measured pressure peaks, which represent the pressure exerted on the plate during the collision. From these we obtained density profiles, and discussed these results in a qualitative way and found that dilation is a function of the vertical coordinate. These results, which show that dilation is approximately constant in the bulk but increases sharply close to the free surface of the layer, are similar to the ones reported in previous works in one and two dimensions [12,13]. We also showed that at a low frequency of excitation, a critical value of $\Gamma\approx2$ exists where a change in the layer dilation takes place. This transition will be discussed in detail in Sec. IV.

IV. PRESSURE AND REFLECTIVITY MEASUREMENTS

Both the time evolution of the pressure, $P(t)$, and the normalized intensity $I(t)/I_o$, are represented in Fig. 9 for two values of Γ when f is in the low frequency regime. For $\Gamma>1$, the layer-plate collision is always visible in the pressure signal as large peaks. However, no trace of this collision is observed in the reflected light up to $\Gamma\sim2$. Thus, for $1<\Gamma<2$, the layer is compact, indicating that the energy in-

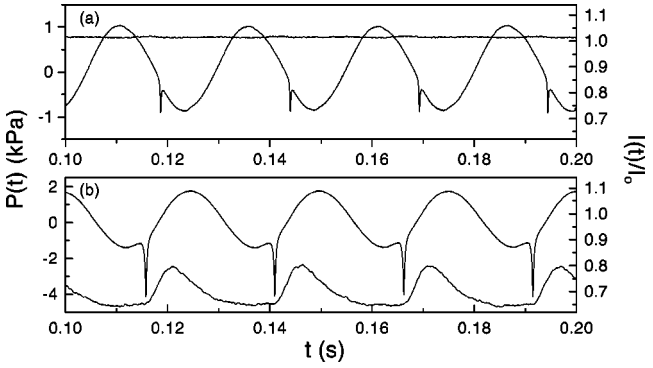

FIG. 9. Time series obtained from pressure and intensity sensors for $f=40$ Hz, (a) $\Gamma=1.2$, and (b) $\Gamma=2.3$.

jected during the layer-plate collision is completely dissipated by the multiple collisions between the grains or by friction. In contrast, for $\Gamma>2$ the time mean value of the reflected light (the dc component) exhibits a strong decrease that shows that the layer undergoes a transition from a compact state to a dilated state. A modulation in time (the ac component) which oscillates at the forcing frequency is also observed in the reflected light for $\Gamma>2$. This modulation is in phase with the pressure peak. Indeed, immediately after the pressure peak occurs, the reflected light increases, indicating that the layer was dilated during the free flight, and that a small compression occurs due to the collision. Furthermore, when the layer takes off, surface dilation starts to increase (a decrease in reflected light).

We first emphasize that this increase in surface dilation is the result of the amplification of small differences in initial conditions, for the free flight of the grains located at the layer surface [14]. Such differences arise as a consequence of the random character of kinetic-energy injection; due to the random packing of grains, a layer plate collision naturally induces velocity fluctuations in the layer. As shown in Fig. 9(b) for $\Gamma>2$, the layer never reaches a compact state, which would correspond to a higher value of the reflected light [see Fig. 9(a)]. This result indicates that the kinetic energy, injected into the internal degrees of freedom of the layer, has not been completely dissipated within the cycle.

To estimate the amount of energy not dissipated, we consider small changes of I in time for early stages of the layer expansion. We can then write

$$I(t)/I_{ref}\approx1-2\Delta\delta_s(t)/[d+\delta_s(0)]. \tag{20}$$

Here $\Delta\delta_s(t)=\delta_s(t)-\delta_s(0)$, and the reference intensity I_{ref} is taken when the layer starts to expand, and corresponds to a finite dilation $\delta_s(0)$ at $t=0$. From the slope of intensity versus time for early stages of the layer expansion, we obtain a characteristic time τ. Dimensionally $\tau^{-1}\sim\Delta V_{to}/[d+\delta_s(0)]$, where ΔV_{to} can be associated with the velocity fluctuations at the taking off time of the particles located at the free surface of the layer. Experimentally, for $2<\Gamma<\Gamma_w$, τ is close to 1/27 s, and is frequency independent. On the other hand, from our intensity measurements we can deduce $\delta_s(0)$, and then obtain an estimate of ΔV_{to}. Our results show that the normalized velocity $\Delta V_{to}/V_c$ increases lin-

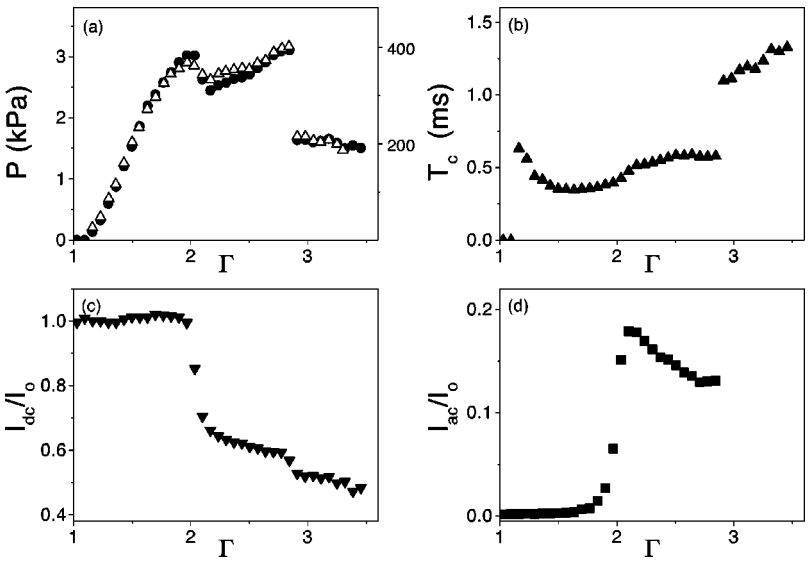

FIG. 10. Maximum pressure P, collision time T_c, and normalized dc and ac components of intensity vs Γ for $f=40$ Hz. In (a) we present the fitting of the maximum pressure P (●), with V_c/T_c (△), whose magnitude is presented in the right axis in units of m/s^2.

early with frequency like $2\times10^{-4}f$, varying from 0.01 for low f ($\sim$35 Hz) to 0.04 for intermediate f ($\sim$200 Hz). Now the feature of typical velocity fluctuations, or ''temperature,'' at the free surface of the layer arises: we note that although most of the energy is dissipated, a small amount of residual ''thermal energy'' is enough to sustain surface dilation.

Concerning the energy injected into the layer during the collisions, we assume that the velocity fluctuations are of order V_c. For a two-dimensional granular layer this point was explored numerically by Labous [15], and his results showed that for short times the injected granular temperature scales as V_c^2. Therefore, our results indicate that the ratio of residual to injection energies, $(\Delta V_{to}/V_c)^2$, increases with f. This allows us to conclude the important fact that the energy dissipation decreases with f. Since $V_c \sim F(\Gamma)/f$, we find that the energy dissipation decreases as the velocity fluctuations decrease. A possible explanation for this is the dependence of the restitution coefficient on the velocity: it was recently shown, in a generalized Hertz theory context, that the resutitution coefficient ϵ scales as $1-av_n^{\alpha}$, where v_n is the relative normal velocity at the collision and a a constant that depends on the elastic and dissipative parameters of the particles [16]. In this work, it was concluded that if the gravity is negligible the parameter α *is positive*, so the collisions become less dissipative as v_n decreases. On the other hand, if the gravity is taken into account, then α is negative and the opposite is true.

We now focus on the transition from a compact state to a dilated state suffered by the layer at $\Gamma\sim2$. Figure 10 illustrates the pressure, P, the collision time, T_c, and the normalized dc (I_{dc}/I_o) and ac (I_{ac}/I_o), components of intensity versus Γ for $f=40$ Hz. P corresponds to the maximum pressure exerted on the plate during the collision, and T_c here is defined as the width of the pressure peak at a quarter of its height. In Fig. 10(a) we also present the numerical fit of P with V_c/T_c; it is evident that $P\sim V_c/T_c$, which is a natural consequence of the impulsive nature of the periodic forcing. At $\Gamma\sim2$, the dc component of the intensity exhibits a strong decrease while its ac component abruptly increases. At the same value of Γ there is a small decrease in the pressure peak, and a small increase in T_c, due to an increase in the bulk dilation in the layer. This decrease in pressure was already observed by Umbanhowar [7], and it is stronger for particles with higher restitution coefficients; however, no correlation with reflectivity measurements was made to investigate the state of the layer. We emphasize that the former transition occurs for $\Gamma<\Gamma_w$. At the onset of surface waves ($\Gamma=\Gamma_w$), the pressure presents a strong decrease associated with the fact that layer-plate collision is spread out in time [7] [Figs. 10(a) and 10(b)].

Using the considerations introduced in previous sections, we calculate δ_b and δ_s as functions of Γ. This is presented in Fig. 11 for $f=40$ Hz. To complete the data, we also present the average dilation $\langle\delta\rangle$, and we observe that the agreement with δ_b is fairly good. Similar to what we found for $\langle\delta\rangle$ (Fig. 8), we observe that both δ_b and δ_s suffer transitions at $\Gamma\approx2$. For $\Gamma<2$ the bulk dilation is higher than the dilation at the surface (which seems to be quite unreal) and δ_s takes negative values. Both facts are due to the choice of $\delta_s=0$ for $I=I_o$. In fact, we ignore the exact value of $\delta_s=\delta_s^o$ for I

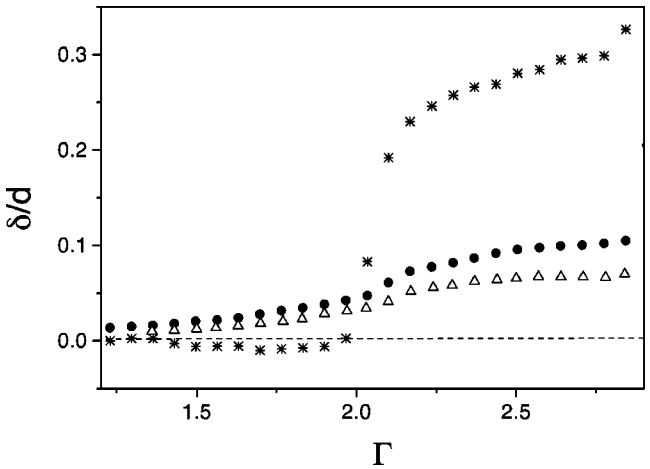

FIG. 11. Bulk dilation δ_b (●), mean dilation $\langle\delta\rangle$ (△), and surface dilation, δ_s (*), vs Γ for $f=40$ Hz.

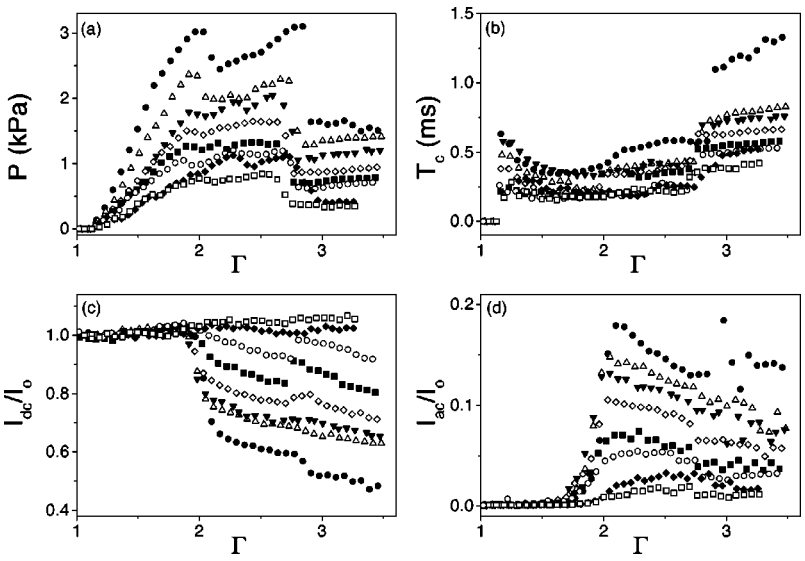

FIG. 12. Maximum pressure P, collision time T_c, and normalized dc and ac components of intensity vs Γ for various values of f: $f=40$ (●), 69 (△), 83 (▼), 111 (◇), 154 (■), 200 (○), 250 (◆), and 350 (□) Hz.

$=I_o$, but we expect it to be small. Thus care must be taken when comparing the bulk and surface dilations, the latter being a reference respect to the initial state. On the other hand, $\delta_s<0$ simply means that the surface layer reaches a state that is more compact than the initial state. This is related to the fact that the initial state, consistent with our experimental method (see Sec. II), is not the most compact packing of the layer.

Thus we say that for $\Gamma<2$ the state of the layer is solidlike, where the injected energy during the collision is dissipated. Nevertheless, in this regime, the available energy is enough to produce a rearrangement of surface grains. In all the cases tested, the maximum compaction was never larger than 2% of the initial density. Consequently, we associate the increase in δ_s and δ_b, observed at low f and $\Gamma>2$ to a solid-liquid-type transition. In the liquid phase, average dilation is large enough to allow particles to move with respect to each other. For low f, at the critical value $\Gamma\approx 2$, the injected energy rate becomes larger than the dissipation rate, and the energy excess sustains the dilation in the granular layer.

In Fig. 12 we include the frequency dependence of the same quantities presented in Fig. 10. As opposed to the case of low f, at high f and for $\Gamma>2$ the dc component of I increases slightly. This indicates that the layer surface has reached a state more compact than the initial one. In this regime, the maximum compaction achieved was about 10% higher than the initial density. It is very important to note that the decrease in pressure associated with the wave instability is clearly observed over the entire range of frequencies [Fig. 12(a)].

Complementing Fig. 12, in Figs. 13(a) and 13(c) we present the maximum pressure and the dc component of I versus f for two values of Γ, both smaller than the critical one for waves, with one right below and the other right above the fluidization transition. Both the maximum pressure and the jump in reflectivity decrease as f increases.

We also present the bulk dilation δ_b [see Fig. 13(b)] calculated directly from the pressure through Eq. (6). We find that δ_b scales as f^b with $b=-1.42\pm0.07$ and $b=-1.54\pm0.03$ for $\Gamma=1.5$ and 2.3, respectively. These values are in very good agreement with those obtained for $\langle\delta\rangle$ [see Fig.

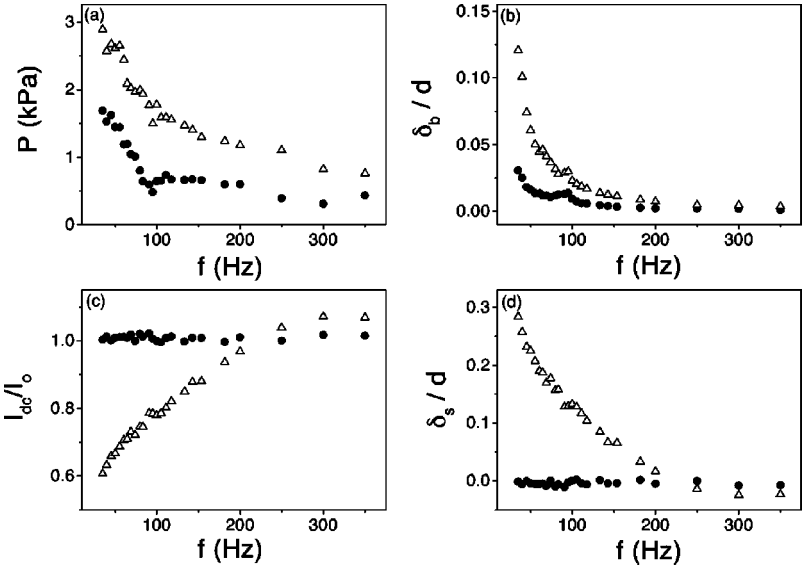

FIG. 13. Maximum pressure P, bulk dilation δ_b, normalized dc component of intensity and surface dilation δ_s vs f for two constant values of Γ below the onset of surface waves: $\Gamma=1.5$ (●), and 2.3 (△). Bulk dilation scales as $\delta_b=af^b$ with $a=0.70\pm0.14$, $b=-1.42\pm0.07$ (●) and $a=1.43\pm0.05$, $b=-1.54\pm0.03$ (△), respectively.

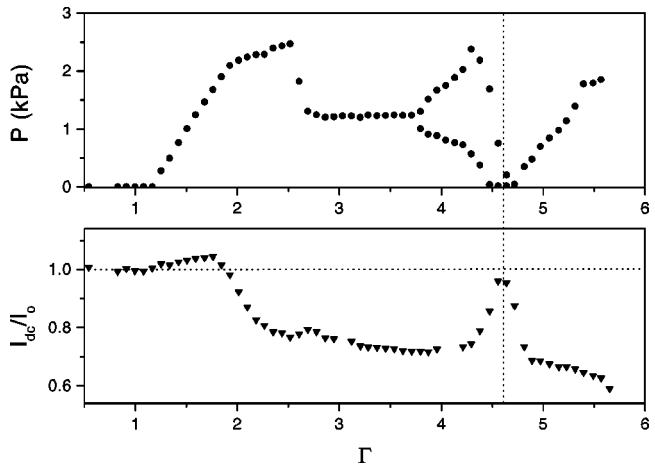

FIG. 14. Maximum pressure P (a) and dc intensity component I_{dc}/I_o (b) as a function of Γ for $f=60$ Hz. The vertical line indicates the flat layer with kinks transition at which $V_c=0$. At $\Gamma \approx 3.6$, as predicted by the inelastic colliding ball model for the center of mass of the layer, a period doubling instability is observed.

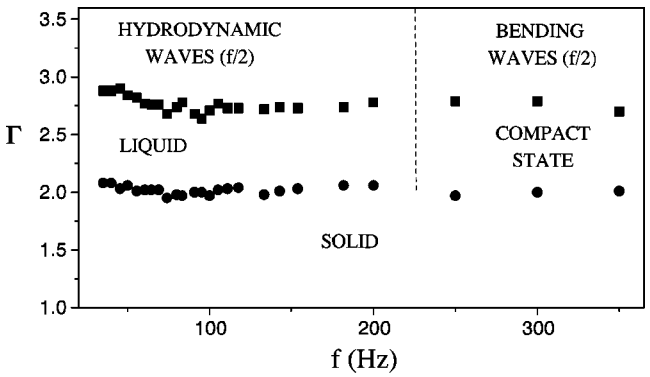

FIG. 15. Phase diagram showing layer state and surface wave transitions. The vertical dashed line at $f=225$ Hz defines the frequency above which the layer strictly undergoes a transition to a state more compact at $\Gamma \sim 2$.

8], and they provide a consistency test for both kinds of measurements. These results indicate that the relevant quantity is not only the ratio of the injected energy per particle to the potential energy required to rise a particle by a fraction of its diameter, in which case δ_b would vary as $1/f^2$, but also the dissipated energy. We note that our results contrast with those obtained by Luding *et al.* in numerical simulations of a column of particles in the completely fluidized regime, where the average dilation scales as $\langle \delta \rangle \sim (Af)^2$, which for Γ constant becomes $\langle \delta \rangle \sim (\Gamma/f)^2$ [12]. However, similar simulations done by the same group for a two-dimensional layer [17] indicated that the layer expansion scales as $h_{cm} - h_{cmo} \sim (Af)^{3/2} \sim (\Gamma/f)^{3/2}$. Even though these results were also obtained in a completely fluidized regime (typically $\Gamma > 10$), we observe quite a good agreement for the *scaling on f* for the expansion of the layer.

On the other hand, information about the surface dilation δ_s versus f is obtained using the intensity data as $I/I_o \approx d^2/(d+\delta_s)^2$ [see Fig. 13(d)]. For $f>225$ Hz, δ_s takes negative values, which indicates that the surface layer is more compact than the initial one. However, in this regime, as shown in Sec. III, the bulk dilation increases with Γ but remains very small: $\delta/d \sim 10^{-3}$.

Finally, let us mention another interesting transition which links to the flat with kink instability reported in previous works [2]. If we increase, Γ further, we find that a period doubling is achieved at $\Gamma \approx 3.6$, as reported before [18,2]. Next, for $\Gamma \approx 4.6$, an inverse transition of the liquid-solid type is detected. Figure 14 shows a typical measurement of both reflected intensity and maximum pressure for a wider range of Γ. We detect that at $\Gamma \approx 4.6$, P strongly decreases, and the mean value of intensity strongly increases. Using the results discussed previously, both changes reflect a strong decrease of grain mobility. We note that the critical value $\Gamma \approx 4.6$ corresponds to $V_c=0$ in the completely inelastic ball model, so in fact no energy is injected into the internal degrees of freedom. We also conclude that no surface waves can be sustained in this regime, except at the kink itself. Indeed, the shear induced at the kink by the flat parts oscillating out of phase is large and enough to induce dilation. At low frequencies, this dilation is enough to allow hydrodynamics waves, like those shown in Fig. 1(c). As Γ is increased further, the pressure increases and the reflectivity decreases. Thus the energy injection again becomes sufficient to sustain surface waves in the layer. This fact is consistent with the existence of $f/4$ waves reported previously [2]. We note that for $\Gamma=4.6$ the maximum velocity of the plate is $Aw \approx 0.12$ m/s; this confirms that the relevant scale of velocity fluctuations is given by V_c and not Aw.

The experimental results presented above can be summarized as follows. Depending on the excitation frequency, we observe different kinds of states and waves. At low frequency, the bulk and surface dilations present strong increases which are associated with a fluidization transition. Surface waves observed in this regime involve relative motion between particles, and are therefore considered as hydrodynamic modes of the layer. At intermediate *f*, although the injected energy is small, we still observe a decrease in reflectivity as a function of Γ. In this regime, as shown in Fig. 13(b), δ_b is too small ($\delta_b/d<0.1$) to allow motion between the particles. Therefore, at the critical Γ, the decrease of reflectivity is the signature of particles fluctuating around their positions at the free surface of the layer. We associate this decrease with a heating up of the solid phase. For higher frequencies, the layer undergoes a compaction crossover which is detected by an increase in the surface density. Below and above this crossover the local bulk dilation δ_b/d is even smaller and is of order 0.005, implying that the mobility in both the bulk and the free surface is completely suppressed. Thus the very low amplitude surface waves, detected in the compaction regime by the strong decrease in the maximum pressure, must correspond to excitations in which the layer is slightly modulated in time and space. We will show in Sec. V that these waves are bending waves, associated with the ability of the compact layer to deform itself. Finally, Fig. 15 presents a phase diagram for the granular layer: phase boundaries separating the various states and sur-

face waves were obtained from the data in Fig. 12. The layer state and surface wave transitions occur for approximately constant values of Γ independent of f.

V. LOW AMPLITUDE WAVES: BENDING WAVES

To check the existence of these waves, we have performed a set of experiments in a two-dimensional granular layer. The advantage of using a two-dimensional system is that this allows us to obtain side views of the waves. This is of particular importance, since bending waves are difficult to visualize as they have amplitudes of the order of 50% of a particle diameter.

In order to observe such small amplitudes, we have used photoelastic cylinders of 6 mm in diameter and 6.35 mm in length. Typical excitation frequencies are about 40 Hz, which for this system are in the high frequency regime. We recall that this regime occurs for frequencies much larger than the frequency crossover $f_d \sim \sqrt{g/d}$. When varying the deepness of the layer (the number of particles is N), this scaling becomes $f_d = \sqrt{g/Nd}$ [19]. In the case of bronze particles of $d \approx 0.12$ mm, bending waves are detected for $f > 225$ Hz. This tells us that these waves should be observed at $f \approx 40$ Hz, for $d = 6$ mm, and for a layer about ten particle diameters thick. With these parameters, for $\Gamma \sim 3.5$, the amplitude of waves should be of the order of 1 mm.

Typical snapshots of two stages of bending waves at $\Gamma = 3.5$, $f = 40$ Hz, and $N = 10$ are presented in Figs. 16(a) and 16(b). We observe that the layer bends slightly with respect to the horizontal. Similar to what occurs for low frequency waves, this modulation alternates in time at half of the frequency forcing (see below). However, in this case, the wavelength of the modulation is about a layer thickness, and is also nearly independent of f. Some particles are marked with black spots which allows us to distinguish them and follow their trajectories [see Figs. 16(a) and 16(b)]. As expected, the mobility of the particles is very low. Only at the surface layer will some particles move with respect to each other over distances of the order of the driving amplitude. In the bulk this motion is completely suppressed.

Additional support for these low amplitude waves is provided in Fig. 16(c), in which a compaction front that moves laterally is observed as a bright zone. This image results from the difference of two consecutive snapshots (the period of acquisition is about 0.8 ms). At a compression zone, the stress in the particles is high so the light is transmitted. Thus the difference of images mainly shows the zones under stress. In the case presented the compression front moves from right to left, and the collision occurs very near the right boundary of the image. In the next cycle the collision occurs near the left boundary and the compression front travels to the right. With a wider view of the layer we observe that in fact two compression fronts are created from each collision point; one front travels in each direction. This kind of visualization allows us to safely say that these parametric waves are also subharmonic, i.e., their frequency is $f/2$. Finally, from the images we estimate the velocity of the compression front of the order of a few meters per second. This value is very high compared to the estimated velocity at the collision

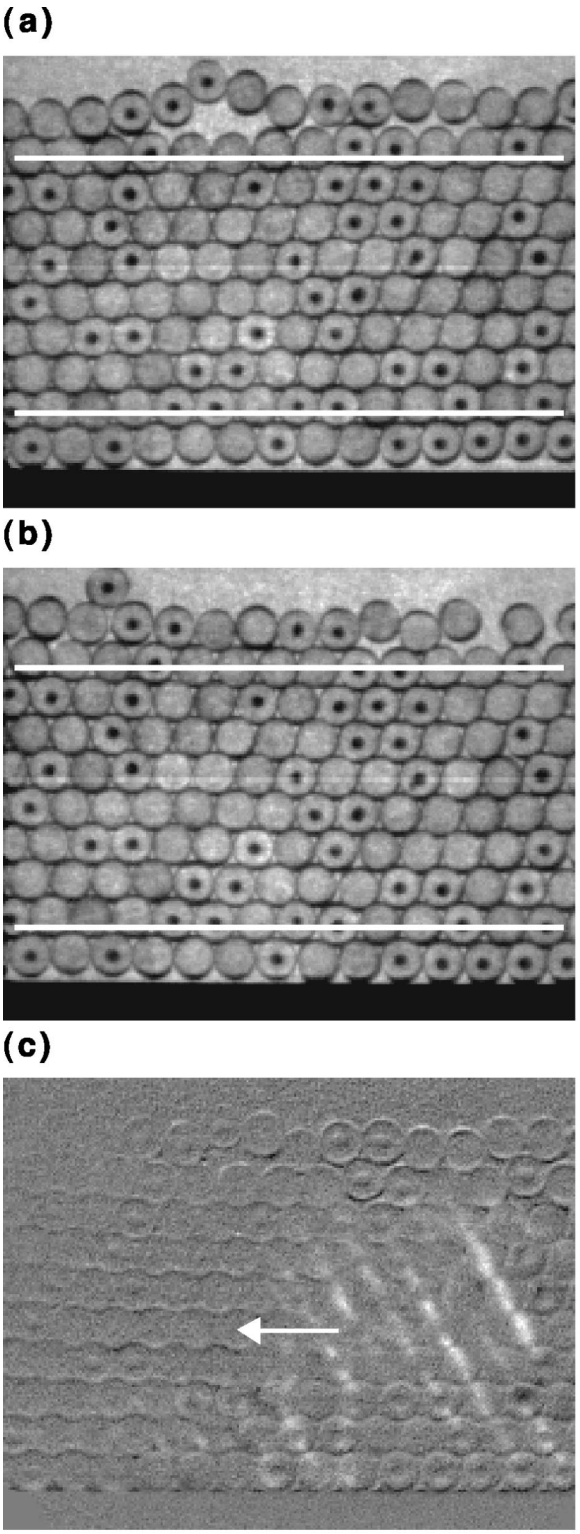

FIG. 16. Typical snapshots of bending waves for $f = 40$ Hz and $\Gamma = 3.6$. In (a) and (b) the white horizontal lines show that the layer bends itself about half a diameter. Both states alternate in time with the frequency of oscillation. In (c) we present the difference of two images during a collision. The bright zones correspond to regions under high stress. In this case the compression front travels to the left.

$V_c \approx 0.25$ m/s; this indicates the existence of contact arcs [see the contact lines in Fig. 16(c)], so, as expected, the average bulk dilation is very small.

VI. CONCLUSIONS

In conclusion, depending on the excitation frequency, we observe different kinds of states and waves. Our experimental results reveal the existence of a solid-liquid-type transition that precedes the subharmonic wave instability. Hydrodynamic surface waves can be then considered as the natural excitations existing in a fluidized granular layer. In contrast, very low amplitude surface waves detected in the compaction regime correspond to excitations in which the layer slightly bends alternatively in time and space. We saw in Sec. V that these waves are in fact associated with the compact character of the layer. The layer states observed and the surface wave transitions occur for approximately constant values of Γ, independent of f.

Additional experimental evidence for the fluidization transition experienced by the layer at $\Gamma \sim 2$ can be found in Ref. [20] (See for instance, Fig. 6 in Ref. [20]). Although they used rather large particles at small forcing frequencies, we find that their experiments are actually in the low frequency regime after estimating the frequency crossover. Independent experimental evidence for the compaction crossover can also be found in previous works. For instance, a strong increase in granular density was found, close to $\Gamma \sim 1.9$, in several experiments on large columns of grains submitted to ''taps'' of a single cycle of vibration [21]. In this case, applying the scaling to the frequency crossover, we found consistently that these experiments correspond to the high frequency limit. Therefore, we conclude that both fluidization as well as compaction transitions are well established experimentally. However, it is still unclear what mechanisms dominate these transitions, and why they arise at a constant value of Γ. We can only safely say that at low energy injection rates, or equivalently at small plate amplitudes with respect to the thickness of the layer, the transition will be of the compaction type. In the opposite case of high energy injections rates, this transition will be of the fluidization type.

We have also shown that for the range of Γ considered, the relevant scale of velocity fluctuations is given by V_c and not Aw. Then, via intensity measurements, we deduced that the dissipation decreases as f increases. This is equivalent to stating that dissipative effects decrease as the velocity fluctuations decrease. As a possible mechanism we noted the dependence of the restitution coefficient on the collisional relative velocity, $\epsilon \sim 1 - a v_n^{\alpha}$. This argument seems plausible if the efective gravity during the collisions is negligible. As the packing of grains is random it is reasonable to expect isotropy in the collisions; then the gravity could be less important. Up to now, we could not conclude about this possible mechanism, and more work should be performed in this direction. As a last remark, as the frequency is increased and the dilation is reduced, we expect that the friction between grains will become an important dissipative mechanism.

Finally, the importance of the bulk and surface dilation measurements is that they provide a complementary way to explore the excitation of the internal degrees of freedom of a vibrated layer. For the dilation in the bulk we have found that, for a constant value of Γ, it is a decreasing function of f of the form $1/f^b$, with $b \approx 3/2$. This agrees with previous simulations of a two-dimensional layer [17]. It is clear that the deviation from the expected value $b=2$ is due to dissipative effects, but the exact numerical value seems to depend on Γ.

ACKNOWLEDGMENTS

It is a pleasure to acknowledge Paul Umbanhowar and Enrique Tirapegui for many enlightening discussions, and Satish Kumar for useful comments on the manuscript. This work was supported by Fondecyt Grant No. 1970682, Catedra Presidencial en Ciencias, and Dicyt USACH.

[1] For recent reviews, see H.M. Jaeger, S.R. Nagel, and R.P. Behringer, Phys. Today **49**(4), 32 (1996); Rev. Mod. Phys. **68**, 1259 (1996).

[2] F. Melo, P. Umbanhowar, and H.L. Swinney, Phys. Rev. Lett. **72**, 172 (1994); **75**, 3838 (1995).

[3] It is well known that the mobility in a granular material depends strongly on the energy injection rate. See, for instance, P.K. Haff, J. Fluid Mech. **134**, 401 (1983).

[4] P. Umbanhowar, F. Melo, and H.L. Swinney, Nature (London) **382**, 793 (1996).

[5] N. Mujica and F. Melo, Phys. Rev. Lett. **80**, 5121 (1998).

[6] H.K. Pak, E. Van Doorn, and R.P. Behringer, Phys. Rev. Lett. **74**, 4643 (1995).

[7] P. Umbanhowar, Ph. D. thesis, University of Texas at Austin, 1996; P. Umbanhowar, F. Melo, and H. L. Swinney, Physica A **288**, 345 (2000).

[8] E. Falcon, C. Laroche, S. Fauve, and C. Coste, Eur. Phys. J. B **5**, 111 (1998).

[9] L. D. Landau and E. M. Lifshitz, *Theory of Elasticity*, 3rd ed. (Pergamon Press, Oxford, 1986), Sec. 9.

[10] Both times T_q and τ_1 depend on the velocity of collision as $V_c^{-1/5}$, and the estimates in the text correspond to the lowest values of V_c achieved in our experiments.

[11] A. Goldshtein, M. Shapiro, and C. Gutfinger, J. Fluid Mech. **316**, 29 (1996).

[12] S. Luding, E. Clement, A. Blumen, J. Rajchenbach, and J. Duran, Phys. Rev. E **49**, 1634 (1994).

[13] E. Clement and J. Rajchenbach, Europhys. Lett. **16**, 139 (1991), J.A.C Gallas, H. Herrmann, and S. Sokolowski, Physica A **189**, 437 (1992).

[14] Simple numerical simulations show that the experimental variation of intensity, during the free flight of the layer, is reproduced by assuming small velocity fluctuations at the take-off time for the particles located at the free surface. Such velocity fluctuations are very close to the ones estimated in the

text [N. Mujica and F. Melo (unpublished)].
[15] L. Labous, Ph. D. thesis, Université Paris VI, 1998.
[16] E. Falcon, C. Laroche, S. Fauve, and C. Coste, Eur. Phys. J. B **3**, 45 (1998).
[17] S. Luding, H. Herrmann, and A. Blumen, Phys. Rev. E **50**, 3100 (1994).
[18] S. Douady, S. Fauve, and C. Laroche, Europhys. Lett. **8**, 621 (1989).
[19] C. Bizon, M.D. Shattuck, J.B. Swift, W.D. McCormick, and H. Swinney, Phys. Rev. Lett. **80**, 57 (1998).
[20] C.E. Brennen, S. Ghosh, and C.R. Wassgren, J. Appl. Mech. **63**, 156 (1996).
[21] J.B. Knight, C.G. Fandrich, Chun Ning Lau, H.M. Jaeger, and S.R. Nagel, Phys. Rev. E **51**, 3957 (1995).